1

Introduction

1.1 Traditional Metallic Biomaterials

Traditional metallic materials have been typically used in medical applications such as orthopedic implants, dental applications, intravascular stents, and prosthetic heart valves. Compared with nonmetallic biomaterials, metallic biomaterials possess superior mechanical properties such as yield strength, ductility, fatigue strength, and fracture toughness [1], which are more suitable for load-bearing without large and/or permanent deformation. Application of metallic biomaterials goes back 100 years; in fact it is reported that a gold (Au) plate was used in the repair of cleft-palate defects as early as in 1565 [2]. Since then, a large number of metals and alloys, such as silver (Ag), platinum (Pt), palladium (Pd), tantalum (Ta), copper (Cu), nickel (Ni), zinc (Zn), aluminum (Al), magnesium (Mg), iron (Fe), carbon steels, stainless steels, cobalt–chromium (Co–Cr) alloys, titanium (Ti) and its alloys, and Nitinol (NiTi alloys), have been introduced into human body [3]. However, practice has shown that most of them are not perfect for implants in the human body due to various factors, such as insufficient mechanical properties, inferior corrosion resistance, and/or inadequate biocompatibility.

More recently, metallic biomaterials with better balance between good mechanical properties, a good corrosion resistance, and an excellent biocompatibility were developed. The common examples of these metallic biomaterials are type 316L stainless steel (316L SS), Co–Cr alloys, and Ti and its alloys [4]. These alloys have been approved for medical devices and surgical implants by the American Society for Testing and Materials (ASTM), and their mechanical properties are listed in Table 1.1. The 316L SS contains 0.03 wt% C, 17–19 wt% Cr, 13–15 wt% Ni, and 2–3 wt% Mo; the high Cr content gives it good resistance to a wide range of corrosive solutions. Due to its relatively low cost, availability, and easy processing, 316L SS has been employed successfully in the human body in contact with tissues and bones for several decades [6]. However, the wear resistance of 316L SS is poor, which makes it less suitable to be used as an artificial joint, because the excessive wear will lead to a rapid loosening. Compared with 316L SS, Co–Cr alloys exhibit a better wear resistance and an excellent corrosion resistance, even in chloride environments [7, 8]. Table 1.1 shows that their mechanical properties are also superior. The range of Co–Cr alloys used in clinical applications includes

Metallic Biomaterials: New Directions and Technologies, First Edition.
Yufeng Zheng, Xiaoxue Xu, Zhigang Xu, Junqiang Wang, and Hong Cai.

Table 1.1 Mechanical properties of traditional metallic biomaterials.

Materials	Elastic modulus (GPa)	Yield strength (MPa)	Tensile strength (MPa)	Elongation (%)	ASTM Standard
Wrought 316L SS	190	190–690	490–1350	12–40	F138
Cast Co–28Cr–6Mo	210–253	450	655	8	F75
Wrought Co–20Cr–15W–10Ni (L605)	210	310–379	860–896	30–45	F90
Wrought Co–35Ni–20Cr–10Mo (MP 35N)	200–300	241–1586	793–1793	8–50	F562
Wrought Co–20Ni–20Cr–3.5Mo–3.5W–5Fe	—	276–1310	600–1586	12–50	F563
CP Ti (grade 1–4)	105	170–483	240–550	15–24	F67
Wrought Ti–6Al–4V ELI	110	760–795	825–860	8–10	F136
Wrought Ti–6Al–4V ELI	110	825–869	895–930	6–10	F1472
Cast Ti–6Al–4V	110	758	860	8	F1108
Wrought Ti–3Al–2.5V	—	517–714	621–862	10–15	F2146
Wrought Ti–6Al–7Nb	105	800	900	10	F1295
Wrought Ti–13Nb–13Zr	79–84	345–725	550–860	8–15	F1713
Wrought Ti–12Mo–6Zr–2Fe	74–85	897	931	12	F1813
Wrought Ti–15Mo	—	483–552	690–724	12–20	F2066
Wrought Ni–Ti	48	—	551	10	F2063

Elastic modulus data from Ref. [4, 5].

wrought and cast alloys. However, the elastic modulus of Co–Cr alloys (220–230 GPa) is similar to that of 316L SS (210 GPa), and both of them are much higher than that of cortical bone (20–30 GPa), leading to stress shielding in the adjacent bone and resulting in a final failure of implantation [3, 4]. Compared with 316L SS and Co–Cr alloys, Ti and its alloys exhibit lower modulus of 55–110 GPa, which is close to the bone. In addition, the passive film of TiO_2 on the surface of Ti and Ti alloys gives them excellent corrosion resistance. Therefore, Ti and its alloys have been selected as the best among the aforementioned traditional metallic biomaterials for its excellent combination of mechanical properties, corrosion resistance, and biocompatibility [9].

1.2 Revolutionizing Metallic Biomaterials and Their New Biofunctions

1.2.1 What are Revolutionizing Metallic Biomaterials?

According to Williams [10], the performance of any biomedical materials is controlled by two characteristics: biofunctionality and biocompatibility. Following this paradigm, many of the metallic materials used in the human body in the past have been extremely limited due to their insufficient biofunctionality and/or inferior biocompatibility [3]. Revolutionizing metallic biomaterials should have not only an excellent biocompatibility but also a specific biofunction in order to match the requirements in a variety of applications. Therefore, the revolutionizing metallic biomaterials researched and developed in recent years have various biofunctions. An interaction between the metallic biomaterials and the host is shown in Figure 1.1.

1.2.2 Antibacterial Function

The most serious complication in implantation surgery is bacterial infection. However, the traditional metallic biomaterials usually do not possess antibacterial function. Therefore, in the past few decades, the bacterial colonization and antibacterial activity on metallic implant materials have been reported under *in vitro* and *in vivo* tests [11–20]. The antibacterial function of metallic biomaterials is based on the antibacterial effect of the alloying elements, such as Ag, Cu, Zn, Co, Ni, Fe, Al, Sn, and Mg [21]. And in the current research of antibacterial metallic biomaterials, Ag and Cu are the commonly used alloying elements.

The metals Ag and Cu have antibacterial functions against a broad spectrum of microorganisms and their effects depend on their doses [22, 23]. The medical uses of Ag include its incorporation into wound dressing and as an antibacterial coating on medical devices. There is little evidence to support the application of wound dressings containing Ag sulfadiazine or Ag nanoparticles for external infections [24–26]. The use of Ag coatings on urinary catheters and endotracheal breathing tubes has been reported [27, 28], which may reduce the incidence of catheter-related urinary tract infections and ventilator-associated pneumonia, respectively. Ag exhibits low toxicity in the human body, and minimal risk is expected due to clinical exposure by inhalation, ingestion, or dermal

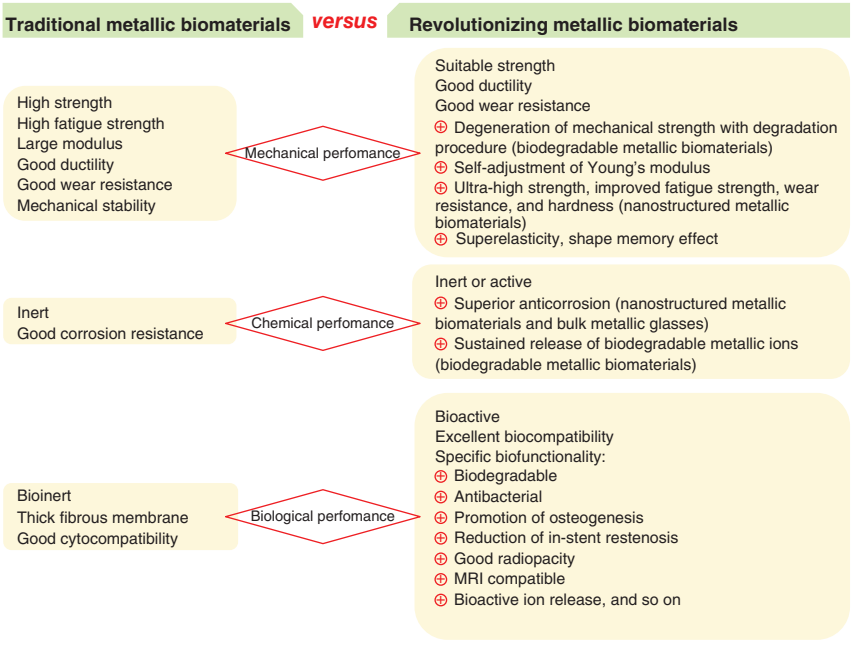

Figure 1.1 Comparison between the traditional and revolutionalizing metallic biomaterials. (Reproduced with permission.)

application [29]. The antibacterial action of Ag is dependent on the Ag ion, which is bioactive and in sufficient concentration readily kills bacteria *in vitro*. Ag and Ag nanoparticles are used as an antibacterial agent in a variety of industrial, healthcare, and domestic applications [30]. However, Ag is not an essential mineral in humans. There is no dietary requirement for Ag, and the chronic intake of Ag products can result in an accumulation of Ag or silver sulfide particles in the skin [31].

Unlike Ag, Cu is a trace metal and an essential component of several enzymes; the adult body contains between 1.4 and 2.1 mg of Cu per kg of body weight [32]. More importantly Cu can be metabolized and is much safer for the human body than Ag. As a matter of fact, in a proper range, the Cu can be excreted in the bile [15]. Cu and its alloys can be considered as natural antibacterial materials [33]. Numerous antibacterial efficacy studies indicated that Cu alloy contact surfaces have natural intrinsic properties to destroy a wide range of bacteria, as well as influenza A virus, adenovirus, and fungi [34]. Some 355 Cu alloys were proven to kill more than 99.9% of disease-causing bacteria within just 2 h when cleaned regularly [35].

Therefore, with comprehensive consideration of the antibacterial characteristic of Ag and Cu, the new antibacterial metallic biomaterials are always focused on the traditional metallic biomaterials containing Ag and/or Cu. There is a large number of studies on Ag- or Cu-bearing antibacterial stainless steels [12–14, 36–46], Ti–Ag or Ti–Cu alloys with antibacterial properties [15, 16, 47, 48], and other antibacterial metallic biomaterials containing Ag or Cu [18–20, 49, 50].

1.2.3 Promotion of Osteogenesis

From the osteogenesis perspective, the aforementioned traditional metallic biomaterials are considered to be bioinert materials. Osseointegration, which is the process of bone healing and the formation of new bone, is the clinical goal of implant surgery. The implant and the bone cells are considered well osseointegrated when new bone cells form, proliferate, and differentiate on the implant [4]. In order to obtain a firm binding between the metallic implants and the surrounding bone, the bioactive interface must facilitate a better bone regeneration and expedited healing. There are many studies that focus on the surface modifications to gain an excellent bone regeneration ability. Some strategies experimented to improve bone integration of metallic implants are development of porous surface, coating of nanoceramic particles, hydroxyapatite coating, oxide coating, and thermal heat treatment of surfaces.

By using rapid prototyping (RP) technique and electrodeposition method, Lopez-Heredia *et al.* [51] have built porous Ti scaffolds with a calcium phosphate (CaP) coating and then studied their osteogenic property. The subcutaneous implantation results showed the presence of mineralized collagen but not mature bone tissue. Even so, the study opened up the possibility of using high-strength porous scaffolds with appropriate osteoconductive and osteogenic properties to reconstruct large skeletal parts in the maxillofacial and orthopedic fields. By using another technique called laser engineered net shaping (LENS™), Balla *et al.* [52] have demonstrated that the modulus of porous Ta can be tailored between 1.5 and 20 GPa by varying its porosity. And the *in vitro* biocompatibility tests showed excellent cellular adherence, growth, and differentiation with abundant extracellular matrix formation on porous Ta structures, which indicated a promotion in biological fixation. On the modified microarc oxidation (MAO)–treated Ti implants surface, fast osteoid deposition comprising high content of Ca, P, C, and N was found in the work of Ma *et al.* [53]. MAO-treated Ti materials have been proved to exhibit good CaP inducement capability *in vivo*, which could accelerate bone tissue growth and shorten the osseointegration time. A highly controlled and reproducible electrochemical polishing process can be used to pattern and structure the surface of Ti–6Al–4V alloy at both the nano- and microscale [54]. The treated surface with a nanoscale TiO_2 layer influenced the program of cellular differentiation culminating in osteogenesis. Chai *et al.* [55] have evaluated the *in vitro* and *in vivo* osteogenesis of a β-tricalcium-phosphate (TCP)-coated Mg alloy. The *in vitro* cell tests showed that the β-TCP coating provided the Mg alloy with a significantly better surface cytocompatibility, and *in vivo* results also confirmed that the β-TCP coating exhibited greatly improved osteoconductivity and osteogenesis in the early 12 weeks postoperative period. To mimic the extracellular microenvironment of bone, Hu *et al.* [56] constructed a bioactive multilayered structure of gelatin/chitosan pair, containing bone morphogenetic protein 2 (BMP2) and fibronectin (FN) on the Ti–6Al–4V surface via a layer-by-layer assembly technique. The *in vivo* tests demonstrated that the multilayer coated Ti–6Al–4V implants promoted the bone density and new bone formation around them after implantation for 4 and 12 weeks, respectively, and showed that the coatings are beneficial for osteogenesis and integration of

implant/bone. In another study, they prepared the apatite/gelatin nanocomposite onto Ti substrates via a coprecipitation method [57]. The results showed that the deposition of apatite/gelatin nanocomposite improved bone density and bone–implant contact rate significantly, and that deposition enhanced the bone osseointegration of Ti-based implants. Bone tissue regeneration in load-bearing regions of the body requires high-strength porous scaffolds capable of supporting angiogenesis and osteogenesis. Gotman *et al.* [58] produced the porous Nitinol scaffolds with a regular 3D architecture resembling trabecular bone using an original reactive vapor infiltration technique. The results of co-culture system of microvascular endothelial cells demonstrated the formation of prevascular structures in trabecular Nitinol scaffolds. It suggested that the strong osteoconductive load-bearing trabecular Nitinol scaffolds could be effective in regenerating damaged or lost bone tissue. Besides the aforementioned methods, Kim *et al.* [59] studied the synergistic effects of nanotopography and co-culture with human umbilical endothelial cells (HUVECs) on osteogenesis of human mesenchymal stem cells (hMSCs). The rational design and fabrication of bone tissue-like nanopatterned matrix are shown in Figure 1.2. Their findings suggested that the nanotopography contributed to the osteogenesis more than co-culture with HUVECs did. However, what is more important than the results is this study provided a new insight on the importance of tissue-inspired nanotopography and co-culture systems in designing engineered platforms for stem cell-based bone tissue engineering, as well as for the fundamental study of stem cell biology. Lee *et al.* [60] studied the bone regeneration around *N*-acetyl

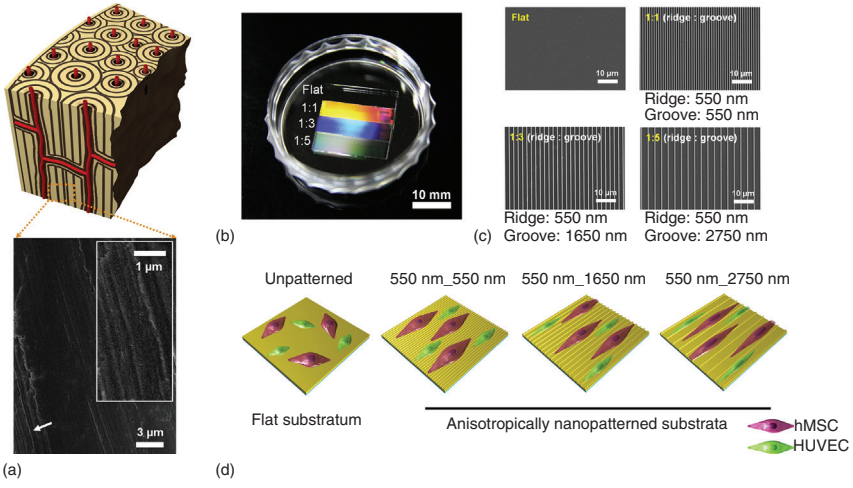

Figure 1.2 Rational design and fabrication of bone tissue-like nanopatterned matrix with various groove sizes. (a) Graphical illustrations and SEM images of *ex vivo* bone tissue. The insert is a high-magnification image of the region indicated by the white arrow, showing the well-aligned nanostructures in bone tissue. (b) A photograph and (c) SEM images of PUA matrix nanotopography on glass slide. The spacing ratio is the ratio of the width to the spacing of nanogrooves. (d) Schematic illustration showing the engineered platforms consisting of hMSCs, HUVECs, and nanopatterned matrix. (Kim *et al.* 2013 [59]. Reproduced with permission of Elsevier.)

cysteine-loaded nanotube Ti (NLN–Ti) dental implant in a rat mandible. The results of μ-computed tomography revealed an increase of newly formed bone volume and bone mineral density in the mandibles of Sprague Dawley rats. The immunohistochemical analysis showed a significantly higher expression of BMP-2, BMP-7, and heme oxygenase-1 and reduced expression of receptor activator of nuclear factor-κB ligand. All the data indicate that NLN–Ti implants enhance osseointegration and highlight the value of the small animal model in assessing diverse biological responses to dental implants.

Mg alloys have been investigated in different fields of medicine and represent a promising biomaterial for implants due to characteristics like bioabsorbability and osteoinduction. Lensing *et al.* [61] tested a bioabsorbable Mg alloy serving as total ossicular replacement prostheses. The *in vivo* results revealed a considerable degradation of implants and obvious bone formation was found 3 months after implantation. Although the Mg alloy corroded before completing the bone reconstruction in time, the increased osteoinduction on the stapes base plate resulted in a tight bone–implant bonding. Therefore, the authors think that the combined application of Mg implant and coating would be a promising solution for improving the bone integration of implants.

In a recent study, Qiao *et al.* [62] reported the stimulation of bone growth following Zn incorporation into biomaterials. Zn is incorporated into the subsurface of TiO_2 coatings (Zn-implanted coatings) by plasma immersion ion implantation and deposition (PIII&D), with the "bulk-doped" coatings prepared by plasma electrolyte oxidation control; the schematic representation of the two Zn incorporation strategies are shown in Figure 1.3. The results revealed that the Zn-implanted coatings resulted in a significant improvement of osteogenesis *in vitro* and *in vivo* compared with the "bulk-doped" coatings. Molecular and cellular osteogenic activities demonstrate that rat BMSCs cultured on the Zn-implanted coatings have higher ALP activity and upregulated osteogenic-related genes (OCN, Col-I, ALP, Runx2). *In vivo* osseointegration studies also showed an early-stage

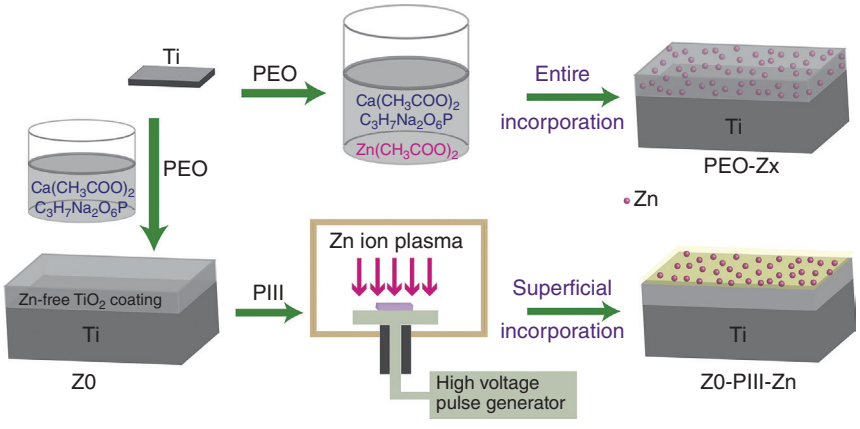

Figure 1.3 Schematic representation of the two Zn incorporation strategies: bulk incorporation and surface incorporation. (Qiao *et al.* 2014 [62]. Reproduced with permission of Elsevier.)

new bone formation and a larger bone contact ratio (12 weeks on the rat model) on the Zn-implanted coating.

1.2.4 Reduction of In-stent Restenosis

Cardiovascular stent materials should possess not only a good cell affinity but also a mechanical property similar to that of blood vessels. Coronary stent implantation has been proven to be an effective technique for the prevention of restenosis in native coronary vessels compared with angioplasty alone. Despite advances in polymer and drug technology, the underlying stent platform remains a key determinant of the clinical outcomes [63]. Currently, the restenosis rates after bare-metal stent (BMS) implantation are still as high as 20–40% at 6 months [64]. Drug-eluting stents (DESs) were shown to be safe and feasible in reducing restenosis [65, 66], but their efficacy and safety have not been confirmed in all clinical settings, especially with regard to treating in-stent restenosis. So reducing the in-stent restenosis remains to be a big challenge. From the angle of biomaterials, the stents should promote the proliferation of vascular endothelial cells (VECs), which hereby accelerate the process of revascularization. In the meantime, they obviously inhibit the proliferation of vascular smooth muscle cells (VSMCs) [17].

Ren *et al.* [67] studied the effect of trace amount of Cu ions released from Cu-bearing stainless steel on reduction of in-stent restenosis. The *in vitro* experimental results proved that this Cu-bearing steel could not only inhibit the proliferation of VSMCs for reducing the formation of thrombosis but also promote the proliferation of VECs needed for the revascularization. However, because there were no *in vivo* experimental results to support it, further animal study should be done.

Over the last 10 years, considerable efforts have been made to develop fully bioresorbable devices called bioresorbable scaffolds (BRSs). BRS technology has gradually matured, and there are numerous devices available, which are currently undergoing preclinical or clinical testing. Mg is an attractive alloy for this concept [68]. The first generation of bioabsorbable metal scaffolds (AMS-1; Biotronik AG, Bülach, Switzerland) was made from a WE43 alloy without drug elution. In porcine coronary arteries, the neointimal tissue proliferation was significantly less in the stented segments with the Mg alloy scaffold as compared with a control group of stainless steel stents [69]. Compared with AMS-1 strut thickness being 165 μm, the strut thickness of DREAMS first generation (DREAMS 1G) was reduced to 120 μm. Moreover, to reduce neointimal growth, the DREAMS was coated with a 1 μm bioresorbable poly(lactide-co-glycolide acid) (PLGA) polymer matrix containing the antiproliferative drug paclitaxel ($0.07\,\mu g\,mm^{-2}$) [70]. Then the DREAMS second generation (DREAMS 2G) with radiopaque markers at both ends (made from Ta) was developed. As a result, DREAMS 2G has slower dismantling and resorption rate. To further reduce the neointima formation, the DREAMS 2G was coated with a bioresorbable polylactic acid polymer (7 μm) featuring sirolimus at a dose of $1.4\,\mu g\,mm^{-2}$. Combining the material characteristics of Mg and the antiproliferative featuring of sirolimus, the DREAMS 2G showed a significant reduction of in-stent restenosis.

1.2.5 MRI Compatibility

Magnetic resonance imaging (MRI) is a technology developed in medical imaging that is probably the most innovative and revolutionary other than computed tomography. MRI has a wide range of applications in medical diagnosis and there are estimated to be over 25 000 scanners in use worldwide [71]. However, most of the currently used implants for cochlear implants, intravascular stents, cardiac pacemakers, and artificial joints are challenged by their unsatisfactory MRI compatibility, because the implants contain ferromagnetic elements [72]. MRI diagnosis is inhibited by the presence of metallic implants, because they become magnetized in the intense magnetic field of the MRI instrument and may produce image artifacts and therefore prevent accurate diagnosis [73, 74]. Hence, improving the MRI compatibility of novel biomedical metallic materials for implants is a very important research topic.

The two trends of development of MRI interventional tools are producing new material with no artifacts and MRI visualizing and guiding of percutaneous devices [75]. Generally, the artifacts affected by MRI decrease with the magnetic susceptibility of the implants [76]. The susceptibilities of selected weakly magnetic metals and alloys are listed in Table 1.2, with water and human tissues as control. In recent years, some studies have focused on the novel MRI-compatible Mg, Zr, and Nb alloys for implants [72, 74, 78–84]. More details can be seen in Section 2.2.

Table 1.2 Susceptibilities of selected weakly magnetic metals and alloys [77].

Materials	Density/ρ (10^3 kg m^{-3})	Susceptibility/χ ($\times 10^{-6}$)
Water (37 °C)	0.933	−9.05
Human tissues	~(1.0 to 1.05)	~(−11.0 to −7.0)
Au	19.32	−34
Cu	8.92	−9.63
Mg	1.74	11.7
Zr	6.49	109
Mo	10.22	123
Ta	16.65	178
Ti	4.54	182
Nb	8.57	237
Pt	21.45	279
Pd	12.02	806
Nitinol (50% Ti, 50% Ni)	6.5	245
Stainless steel (nonmagnetic, austenitic)	8.0	3520–6700

Source: Reproduced with permission of The American Society of Physicist Medicine.

1.2.6 Radiopacity

Radiopacity is an important property of medical devices such as vascular stents and catheters during placement and deployment. Especially in cardiovascular stents, it is essential to monitor the catheter's progression in the vascular branches under an X-ray fluoroscopy, therefore, avoiding invasive procedures on patients [75]. Usually, the absorption of X-rays depends on the number of protons of the elements being used, and the metals with higher X-ray absorption coefficient will become more radiopaque during the interventional operation. There are various methods to improve radiopacity, such as alloying, coating, banding, and addition of contrast agents [85]. In order to obtain the optimal comprehensive performance, the researchers pay more attention to the stent materials and coatings. More details can be found in Section 2.3.

1.2.7 Self-Adjustment of Young's Modulus for Spinal Fixation Applications

The implantation of metallic rods plays an important role in the treatment of spinal diseases and conditions such as scoliosis, spondylolisthesis, and spinal fractures [86]. Due to the special function of the spine, an implant with a higher Young's modulus is expected from the viewpoint of surgeons for better workability during operation, while a lower Young's modulus is desired from the viewpoint of patients for preventing stress shielding effects. Therefore, if there existed any metallic biomaterials with changeable Young's modulus, the conflicting requirements between surgeons and patients may be satisfied at the same time.

Based on this purpose, Nakai *et al.* [87] proposed a solution to satisfy this conflicting requirement. For certain metastable β-type Ti alloys, a nonequilibrium phase, such as α′, α″, or ω, appears during deformation. If the deformation-induced phase shows a higher Young's modulus than the matrix, the Young's modulus of the deformed part increases, while that of the nondeformed part remains low. Thus the springback can be suppressed by deformation-induced phase transformation during bending in the course of surgery, and a low Young's modulus can be retained for the benefit of the patient, as can be seen in Figure 1.4. Besides, their group studied the Ti–Zr, Ti–Mo, and Ti–Cr alloys with changeable Young's moduli for spinal fixation applications [88–91]. The results showed that the Ti–30Zr–3Cr–3Mo, Ti–17Mo, and Ti–12Cr alloys were promising candidates for spinal fixation applications.

1.3 Technical Consideration on Alloying Design of Revolutionizing Metallic Biomaterials

1.3.1 Evolution of Mechanical Properties with Implantation Time

For many decades, the traditional metallic biomaterials have always been used extensively for surgical implants due to good formability, high strength, and high resistance to fracture. However, the surgical implants fabricated with these traditional metallic biomaterials are permanent implants, due to their bioinert

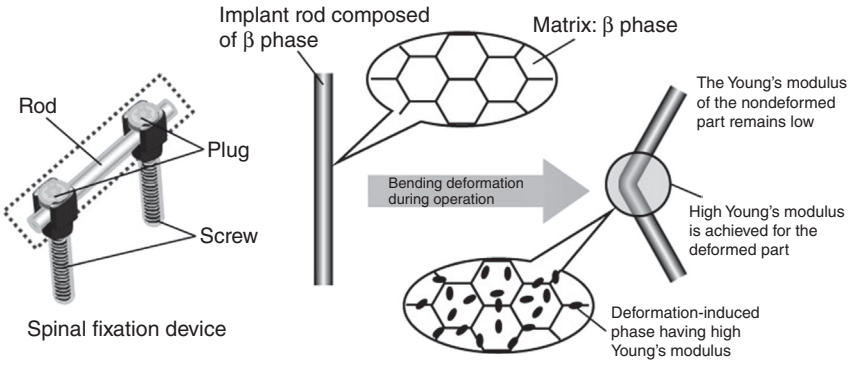

Figure 1.4 Concept of changeable Young's modulus of implant rods during surgery. (Nakai *et al.* 2011 [87]. Reproduced with permission of Elsevier.)

characteristics. Therefore, during their service, their mechanical properties were hardly changed with the prolongation of implantation time. But sometimes the implantation failure would occur because these traditional metallic biomaterials, which have much higher stiffness than bone, prevent the needed stress being transferred to adjacent bone, resulting in bone resorption around the implant and consequently to implant loosening [92].

With the advance of biomaterials science, the new biomaterials possess more matchable properties to human tissues than ever before. Their stiffness, strength, and fracture toughness are shown in Figure 1.5 [93]. Table 1.3 also lists the mechanical properties of some revolutionizing metallic biomaterials with various biofunctions.

Revolutionizing metallic biomaterials not only possess unique biofunctionality but also feature capability to evolve their mechanical properties during their implantation time. Over recent years, a new class of metallic biomaterials named as biodegradable metals (BMs) has been widely studied by materials scientists. The BMs are expected to corrode gradually *in vivo*, with an appropriate host response elicited by released corrosion products, and then dissolve completely upon fulfilling the mission to assist with tissue healing with no implant residues [100]. Two classes of BMs have been proposed: Mg- and Fe-based alloys. They are envisaged in three targeted applications: orthopedic, cardiovascular, and pediatric implants. Given that the BMs are prone to corrode in human body environment, the mechanical integrity of BMs would change with the implantation time, as shown in Figure 1.6. During the first 2–3 weeks postfracture, the soft callus forms, which corresponds roughly to the time when the fragments are no longer moving freely. This early soft callus can resist compression but shows tensile properties similar to the fibrous tissue of which the ultimate tensile strength and elongation at rupture are 4–19 MPa and 10–12.8%, respectively [101]. Hence the mineralization of the soft callus proceeds from the fragment ends toward the center of the fracture site and forms a hard callus, which has regained enough strength and rigidity to allow low-impact exercise at the end of the repair phases [101, 102]. The time to achieve the hard bone union varies greatly according to the fracture configuration and location, status of the adjacent

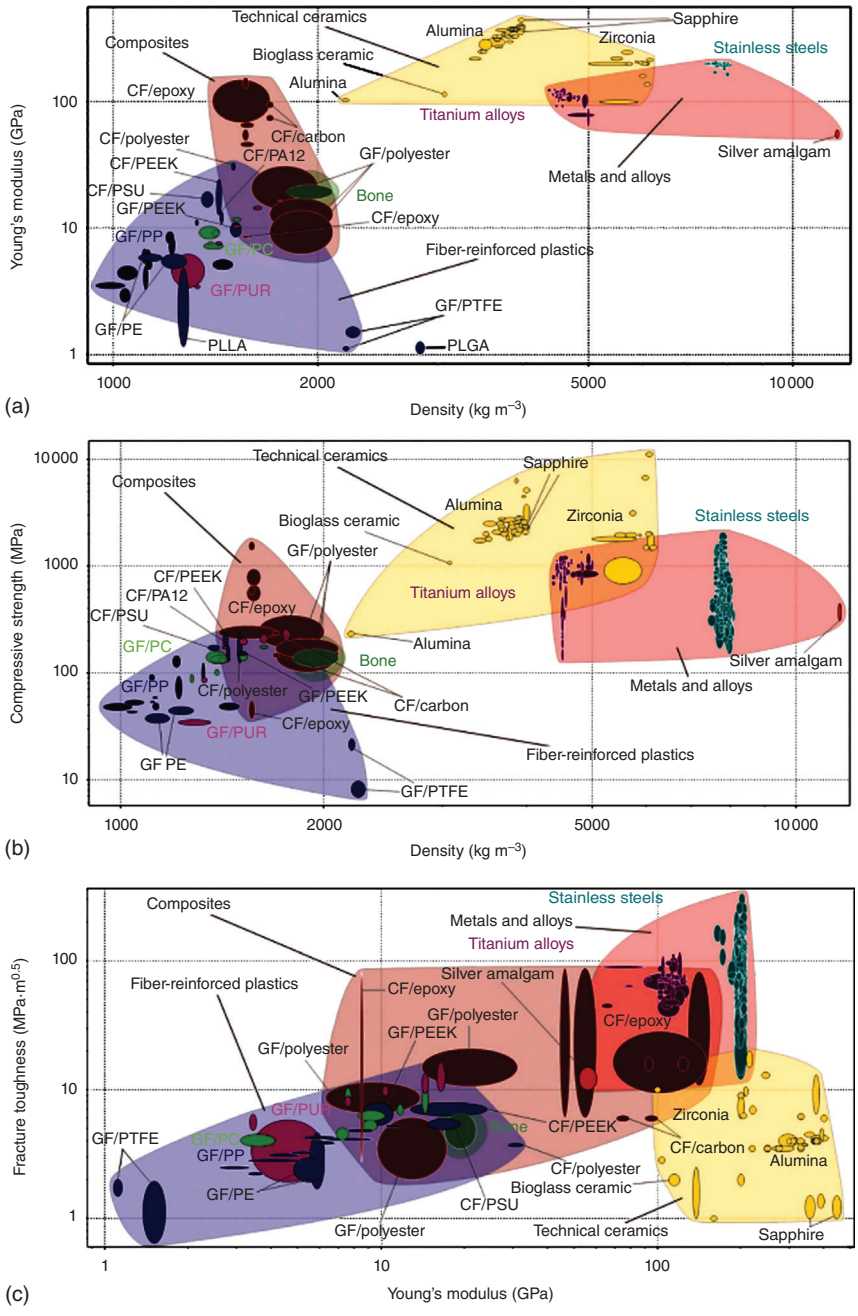

Figure 1.5 Comparison of (a) stiffness, (b) strength, and (c) fracture toughness for metals, technical ceramics, composites, and fiber-reinforced plastic with respect to bone. CF, carbon fiber; GF, glass fiber; PA12, polyamide12; PC, polycarbonate; PE, polyethylene; PEEK, poly ether ether ketone; PLGA, poly(lactide-co-glycolide acid); PLLA, poly(L-lactic acid; PP, polypropylene; PSU, polysulfone; PTTE, polytetrafluoroethylene; and PUR, polyurethane. (Mantripragada *et al.* 2013 [93]. Reproduced with permission of John Wiley & Sons.)

Table 1.3 Comparison of mechanical properties between some revolutionizing and traditional metallic biomaterials.

Elastic modulus (GPa)	Microhardness (HV)	Yield strength (MPa)	Ultimate tensile strength (MPa)	Elongation (%)	Biofunctional improved property	References
19.9 ± 1.8	52.7–76.4	107.9 ± 12.3	—	—	—	[94, 95]
190	—	190–690	490–1350	12–40	—	ASTM F138
—	142–154	255–285	562–593	58–68	Antibacterial	[37]
—	—	—	—	—	Antibacterial	[44]
—	—	850–1480	900–1560	17–30	Enhanced mechanical and fatigue properties	[96]
105	—	170–483	240–550	15–24	—	ASTM F67
—	—	640	710	14	Enhanced mechanical properties	[97]
—	—	790	950	14	Enhanced mechanical properties	[98]
110	—	760–795	825–860	8–10	—	ASTM F136
—	—	1310	1370	12	Enhanced fatigue properties	[99]
68–79	—	650–770	800–1000	8–18	Self-adjustment of Young's modulus	[88]
73–84	—	500–730	725–850	15–25	Self-adjustment of Young's modulus	[89]
—	—	—	710	17.6	Shape memory effect, superelasticity, and antibacterial	[18]
44–46	27–43	—	165–210	13–20	Biodegradable, antibacterial	[19]
—	—	—	—	—	Biodegradable, antibacterial	[20]
1.5–20	—	—	—	—	Promote enhanced/early biological fixation	[52]

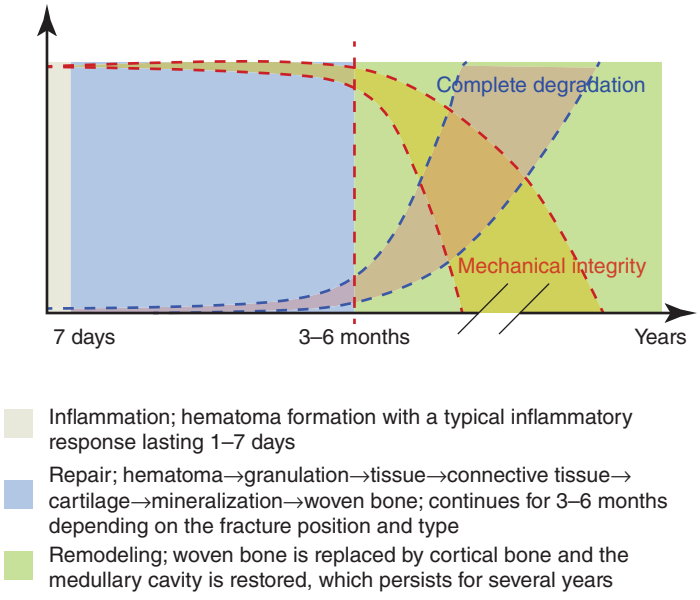

Figure 1.6 The schematic diagram of the degradation behavior and the change of mechanical integrity of BM implants during the bone healing process. (Zheng *et al.* 2014 [100]. Reproduced with permission of Elsevier.)

soft tissues, and patient characteristics (e.g., age, health status, concurrent injuries/diseases). According to Perkin's classification of fracture healing, a spiral fracture in the upper limb unites in 3 weeks and consolidates in 6 weeks. The fracture healing time doubles for a transverse fracture and doubles again for the lower limb. As can be seen in Figure 1.7, the mechanical support should be sustained for 12–24 weeks depending on the clinical conditions.

Currently, the reported Mg alloy stents and bone implants indicate a relatively faster degeneration of mechanical properties before/during the tissue remodeling process than expected. For example, the reported Mg-based BM stents completely degraded within 4 months and the mechanical integrity of the stent was lost much faster than predicted. In the future, surface coating could be used as a remedy to extend the mechanical integrity of Mg-based BM stents. In the case of Fe-based BM stents, they exhibit good mechanical support during 4 months, and much slower loss of mechanical integrity of stent occurs. In the near future, research should consider how to control the speed of biodegradation.

1.3.2 Biocorrosion or Biodegradation Behavior and Control on Ion Release

For traditional metallic biomaterials, good corrosion resistance is one of the major factors determining their biocompatibility. When they are implanted in the human body, a highly electrolytic environment, implants become the site of electrochemical reactions and lead to the release of metal ions into the surrounding tissues [103]. The traditional metallic biomaterials are prone to release metal ions

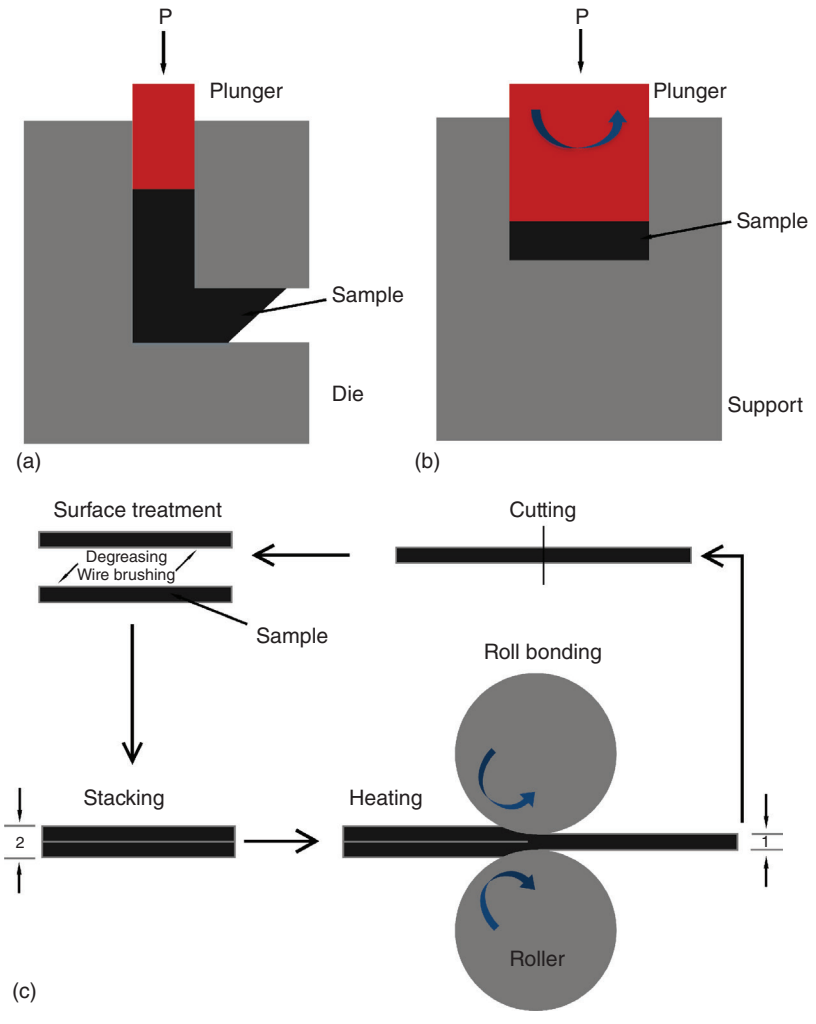

Figure 1.7 Schematic illustration of (a) ECAP, (b) HPT, and (c) ARB. (Reproduced with permission.)

such as Ni, Cr, Co, Al, and V ions, which might have toxic, allergic, and potentially carcinogenic effects [104–108]. The good news is that these traditional metallic biomaterials are chemically inert and highly corrosion resistant; all of these ions released into human body would be minimal. The comparison of *in vitro* corrosion properties between some revolutionizing metallic biomaterials and traditional metallic biomaterials is shown in Table 1.4.

Compared with traditional metallic biomaterials, the BMs, such as Mg alloys, Fe alloys, and Zn alloys, are expected to be totally degraded in the body and their biocorrosion products to be nondeleterious to the surrounding tissues. The biocompatibility and biodegradability of Mg-based alloys have attracted increasing attention as candidate materials for degradable coronary stents [114–116]. Biodegradable stents have not yet entered clinical practice, but results from early

Table 1.4 Comparison of *in vitro* corrosion properties between some revolutionizing and traditional metallic biomaterials.

Materials	Solutions	V_{corr} (V)	I_{corr} (μA cm^{-2})	v_{corr} (mm yr^{-1})	References
Pure Ti	Artificial saliva	−0.343	0.698	0.311	[109]
Co–Cr	Artificial saliva	−0.208	0.479	0.214	
Ni–Cr	Artificial saliva	−0.173	0.198	0.088	
TiNb	Artificial saliva	−0.02	0.3	0.001	[110]
TiNi	Artificial saliva	−0.15	3.5	0.030	
TiNiCu	Artificial saliva	−0.14	2.5	0.022	
Ti–6Al–4V	Hank's	−0.407	0.019	—	[111]
Ti–6Al–7Nb	Hank's	−0.368	0.053	—	
Ti–13Nb–13Zr	Hank's	−0.374	0.028	—	
316L SS	Ringer's	−0.195	0.218	—	[112]
Mg (rolled)	SBF	−1.796	37.24	0.84	[113]
Mg–1Al	SBF	−1.685	136.80	3.09	
Mg–1Ag	SBF	−1.708	53.95	1.22	
Mg–1In	SBF	−1.863	42.96	0.96	
Mg–1Mn	SBF	−1.825	20.15	0.45	
Mg–1Si	SBF	−1.634	28.36	0.64	
Mg–1Sn	SBF	−1.787	54.84	1.24	
Mg–1Y	SBF	−1.848	73.06	1.65	
Mg–1Zn	SBF	−1.805	40.78	0.92	
Mg–1Zr	SBF	−1.633	40.20	0.91	

studies have shown their feasibility [117, 118] and generated a high level of expectations for physicians, patients, industrialists, and researchers. The most recent clinical advances reported relate to the use of biodegradable stents made of Mg-based alloys to treat two cases of congenital heart disease in babies [119, 120] and to treat critical limb ischemia cases in adults [121, 122]. Furthermore, a nonrandomized multicenter clinical trial of Mg-based alloy stents for treating coronary artery disease in adults was recently conducted [69]. The results seem encouraging. However, the stents were made of coarse-grained WE43 alloy and still corroded too fast: they lasted no more than 4 months. Moreover, WE43 contains too much rare earth elements (7 wt%), which may be a toxicological concern.

1.4 Novel Process Technologies for Revolutionizing Metallic Biomaterials

The revolutionizing metallic biomaterials have also been developed by new techniques except for new material designs.

1.4.1 3D Printing

Additive manufacturing (AM) technology, usually referred to 3D printing, has been gaining great attention for directly fabricating biodevices with structures or properties similar to those of natural body tissues. AM shows incomparable advantage in customizing complex, functional, and personalized tissue engineering scaffolds with respect to conventional manufacturing approaches of casting, milling, and sintering [123]. The 3D printing is an RP technology, which is used to create complex three-dimensional parts directly from a computer model of the part, with no need for tooling [124, 125]. 3D printing is also an RP technology that has been used to process BRSs for tissue engineering applications [126]. The technology is based on the printing of a binder through a print head nozzle onto a powder bed, with no tooling required. The part is built sequentially in layers: The binder is delivered to the powder bed producing the first layer, the bed is then lowered to a fixed distance, powder is deposited and spread evenly across the bed, and a second layer is built. This is repeated until the entire part, for example, a porous scaffold, is fabricated. Following the treatment, the object is retrieved from the powder bed and excess unbound powder is removed. The speed, flow rate, and even drop position can be computer controlled to produce complex 3D objects. This printing technique permits CAD and custom-made fabrication of bioresorbable hybrid scaffold systems. The entire process is performed under room-temperature conditions. Hence, this technology has great potential in tissue engineering applications. Biological agents, such as cells, growth factors, and so on, can be incorporated into a porous scaffold without inactivation if nontoxic binders such as water can be used [127]. Unfortunately, aliphatic polyesters can be dissolved only in highly toxic solvents, such as chloroform and methylene chloride. To date, only BRSs without biological agents within the polymer matrix and in combination with particle leaching have been processed by 3D printing. In addition, the mechanical properties and accuracy of the specimen manufactured by 3D printing have to be significantly improved.

1.4.2 Safety and Effectiveness of Biofunctions

Interactions in the biological environment are extremely complex. A material's biocompatibility may change depending solely on where in the body it is utilized and the role it is expected to perform. When designing the appropriate metallic biomaterials, one should ask the following questions: whether the element is known for adverse effects to the biological process; whether the metal is carcinogenic (cancer causing), mutagenic (mutation causing), genotoxic (DNA damaging), or cytotoxic (cell destructing/killing); whether it incites an allergic response; and whether it can resist the corrosive biological environment. Though an individual metal's answers cannot conclusively determine the final alloy's biocompatibility, answering these questions can at least allow reasonable predictions of how the material is going to perform in its environment. Biesiekierski *et al.* [128] briefly summarized the biological impact of 3d, 4d, and 5d transition metals; it can be seen that Ti, Au, Sn, Ta, Nb, Ru, and Zr can be classed as highly biocompatible. Hf and Re hold promise for further research but must be studied carefully. All other elements reviewed are considered less satisfactory, as listed in Table 1.5.

Table 1.5 Biological impact: red indicates a serious concern; yellow indicates a moderate concern; and green indicates minimal/no concern.

Periodic position	Element	Biocompatible	Carcinogenic	Genotoxic	Mutagenic	Cytotoxic	Allergenic	Prone to corrosion	Other[a]
3d	Ti	Yes	No	No	No	Med	No	No	No
	V	No	Yes	Yes	Yes	High	Disputed	No	No
	Cr	No	Disputed	Yes	Yes	High	Yes	No	No
	Mn	No	No	Yes	No	High	No	Yes	No
	Fe	No	No	Yes	Disputed	Med	No	Yes	No
	Co	No	Yes	Yes	Yes	High	Yes	Yes	Yes
	Ni	No	Yes	Yes	Yes	High	Yes	Yes	Yes
	Cu	No	No	Yes	Yes	High	Yes	Yes	Yes
4d	Zr	Yes	No	No	No	Low	No	No	No
	Nb	Yes	No	No	No	Low	No	No	No
	Mo	No	Disputed	Yes	Yes	Low	Yes	Yes	Yes
	Tc	No	Radioactive						
	Ru	Yes	No	No	No	Med	No	No	Yes
	Rh	No	Yes	Yes	Yes	High	Unknown	No	No
	Pd	No	Yes	No	Disputed	Med	Yes	No	No
	Ag	No	No	No	No	High	Yes	No	Yes

5d	Hf	Unknown	Unknown	Unknown	Unknown	Med	No	No	Unknown
	Ta	Yes	No	No	No	Low	No	No	No
	W	No	Yes	Yes	No	Med	No	Yes	No
	Re	Unknown	Unknown	Unknown	Unknown	Unknown	No	No	Unknown
	Os	No	Unknown	Yes	Yes	High	No	Yes	No
	Ir	No	No	No	Yes	High	No	No	Yes
	Pt	No	Yes	Yes	Yes	High	Yes	No	No
	Au	Yes	No	No	No	High	No	No	No
Other	Al	No	No	Yes	No	Low	No	No	Yes
	Zn	No	No	No	No	High	No	No	Yes
	Sn	Yes	No	No	No	Low	No	No	Yes

Source: Biesiekierski *et al.* 2012 [128]. Reproduced with permission of Elsevier.

a) Refers to issues beyond those already listed. For example, hemolysis, neurological effects.

1.4.3 Severe Plastic Deformation

Although the mechanical and physical properties of all crystalline materials are determined by several factors, the average grain size of the material generally plays a very significant and often a dominant role. Accordingly, attention has been directed toward the development of severe plastic deformation (SPD) techniques that may be used to fabricate ultrafine-grained (UFG) materials with grain sizes in the submicrometer and nanometer range [129], such as equal channel angular pressing (ECAP) [130–132], high-pressure torsion (HPT) [133–136], and accumulative roll-bonding (ARB) [137–140]. These methods could always improve the strength and ductility of alloys simultaneously. The schematic illustrations of these methods are shown in Figure 1.7.

Among these three SPD methods, ECAP is the most promising technique that can process bulk UFG materials large enough for structural applications. However, the grain refinement during the ECAP process is affected by accumulative strain and the interaction of shearing plane with crystal structure and deformation texture. Compared with ECAP, there is experimental evidence suggesting that greater grain refinement may be achieved using HPT. In the ARB method, stacking of materials and conventional roll-bonding are repeated in the process, as can be seen in Figure 1.6c. After several cycles of ARB, ultrafine (submicron) grain structure with large misorientations, that is, polycrystal, was formed and the materials were strengthened dramatically [141].

References

1 Pilliar, R.M. (2009) in *Biomedical Materials* (ed. R. Narayan), Springer, New York, pp. 41–82.
2 Ludwigso, D.C. (1965) Requirements for metallic surgical implants and prosthetic devices. *Met. Eng. Q.*, **5** (3), 1–7.
3 Gotman, I. (1997) Characteristics of metals used in implants. *J. Endourol.*, **11** (6), 383–389.
4 Geetha, M., Singh, A.K., Asokamani, R., and Gogia, A.K. (2009) Ti based biomaterials, the ultimate choice for orthopaedic implants – a review. *Prog. Mater Sci.*, **54** (3), 397–425.
5 Milošev, I. (2010) Metallic materials for biomedical applications: laboratory and clinical studies. *Pure Appl. Chem.*, **83** (2), 309–324.
6 Navarro, M., Michiardi, A., Castano, O., and Planell, J.A. (2008) Biomaterials in orthopaedics. *J. R. Soc. Interface*, **5** (27), 1137–1158.
7 McKee, G.K. and Watson-Farrar, J. (1966) Replacement of arthritic hips by the McKee-Farrar prosthesis. *J. Bone Joint Surg. Br.*, **48** (2), 245–259.
8 Songur, M., Celikkan, H., Gokmese, F., Simsek, S.A., Altun, N.S., and Aksu, M.L. (2009) Electrochemical corrosion properties of metal alloys used in orthopaedic implants. *J. Appl. Electrochem.*, **39** (8), 1259–1265.
9 Niinomi, M., Nakai, M., and Hieda, J. (2012) Development of new metallic alloys for biomedical applications. *Acta Biomater.*, **8** (11), 3888–3903.
10 Williams, D.F. (1992) in *Materials Science and Technology*, vol. **14** (eds R.W. Cahn, P. Haasen, and E.J. Kramer), Wiley-VCH, Weinheim, pp. 1–27.

11 Bosetti, M., Masse, A., Tobin, E., and Cannas, M. (2002) Silver coated materials for external fixation devices: in vitro biocompatibility and genotoxicity. *Biomaterials*, **23** (3), 887–892.

12 Dan, Z.G., Ni, H.W., Xu, B.F., Xiong, J., and Xiong, P.Y. (2005) Microstructure and antibacterial properties of AISI 420 stainless steel implanted by copper ions. *Thin Solid Films*, **492** (1–2), 93–100.

13 Chiang, W.-C., Tseng, I.S., Moller, P., Hilbert, L.R., Tolker-Nielsen, T., and Wu, J.-K. (2010) Influence of silver additions to type 316 stainless steels on bacterial inhibition, mechanical properties, and corrosion resistance. *Mater. Chem. Phys.*, **119** (1-2), 123–130.

14 Hong, I.T. and Koo, C.H. (2005) Antibacterial properties, corrosion resistance and mechanical properties of Cu-modified SUS 304 stainless steel. *Mater. Sci. Eng., A*, **393** (1–2), 213–222.

15 Shirai, T., Tsuchiya, H., Shimizu, T., Ohtani, K., Zen, Y., and Tomita, K. (2009) Prevention of pin tract infection with titanium-copper alloys. *J. Biomed. Mater. Res. Part B*, **91B** (1), 373–380.

16 Liu, J., Li, F., Liu, C., Wang, H., Ren, B., Yang, K. *et al.* (2014) Effect of Cu content on the antibacterial activity of titanium-copper sintered alloys. *Mater. Sci. Eng., C*, **35**, 392–400.

17 Ren, L. and Yang, K. (2013) Bio-functional design for metal implants, a new concept for development of metallic biomaterials. *J. Mater. Sci. Technol.*, **29** (11), 1005–1010.

18 Zheng, Y.F., Zhang, B.B., Wang, B.L., Wang, Y.B., Li, L., Yang, Q.B. *et al.* (2011) Introduction of antibacterial function into biomedical TiNi shape memory alloy by the addition of element Ag. *Acta Biomater.*, **7** (6), 2758–2767.

19 Tie, D., Feyerabend, F., Mueller, W.-D., Schade, R., Liefeith, K., Kainer, K.U. *et al.* (2013) Antibacterial biodegradable Mg-Ag alloys. *Eur. Cells Mater.*, **25**, 284–298.

20 Lock, J.Y., Wyatt, E., Upadhyayula, S., Whall, A., Nunez, V., Vullev, V.I. *et al.* (2014) Degradation and antibacterial properties of magnesium alloys in artificial urine for potential resorbable ureteral stent applications. *J. Biomed. Mater. Res. A*, **102** (3), 781–792.

21 Berry, C.W., Moore, T.J., Safar, J.A., Henry, C.A., and Wagner, M.J. (1992) Antibacterial activity of dental implant metals. *Implant Dent.*, **1** (1), 59–65.

22 Agarwal, A., Weis, T.L., Schurr, M.J., Faith, N.G., Czuprynski, C.J., McAnulty, J.F. *et al.* (2010) Surfaces modified with nanometer-thick silver-impregnated polymeric films that kill bacteria but support growth of mammalian cells. *Biomaterials*, **31** (4), 680–690.

23 Kishimoto, T., Fukuzawa, Y., Abe, M., Hashimoto, M., Ohno, M., and Tada, M. (1992) Injury to cultured human vascular endothelial cells by copper (CuSO4). *Nihon Eiseigaku Zasshi*, **47** (5), 965–970.

24 Atiyeh, B.S., Costagliola, M., Hayek, S.N., and Dibo, S.A. (2007) Effect of silver on burn wound infection control and healing: review of the literature. *Burns*, **33** (2), 139–148.

25 Hermans, M.H. (2006) Silver-containing dressings and the need for evidence. *Am. J. Nurs.*, **106** (12), 60–68.

26 Storm-Versloot, M.N., Vos, C.G., Ubbink, D.T., and Vermeulen, H. (2010) Topical silver for preventing wound infection. *Cochrane Database Syst. Rev.*, **17** (3), CD006478.

27 Beattie, M. and Taylor, J. (2011) Silver alloy vs. uncoated urinary catheters: a systematic review of the literature. *J. Clin. Nurs.*, **20** (15-16), 2098–2108.

28 Bouadma, L., Wolff, M., and Lucet, J.C. (2012) Ventilator-associated pneumonia and its prevention. *Curr. Opin. Infect. Dis.*, **25** (4), 395–404.

29 Lansdown, A. (2006) Silver in health care: antimicrobial effects and safety in use. *Curr. Prob. Dermatol.*, **33**, 17–34.

30 Maillard, J.Y. and Hartemann, P. (2013) Silver as an antimicrobial: facts and gaps in knowledge. *Crit. Rev. Microbiol.*, **39** (4), 373–383.

31 Fung, M.C. and Bowen, D.L. (1996) Silver products for medical indications: risk-benefit assessment. *J. Toxicol. Clin Toxicol.*, **34** (1), 119–126.

32 Copper Development Association Inc. Copper in Human Health, http://www.copper.org/consumers/health/cu_health_uk.html (accessed 14 November 2016).

33 Dollwet, H.H.A. and Sorenson, J.R.J. (1985) Historic uses of copper-compounds in medicine. *Trace Elem. Med.*, **2** (2), 80–87.

34 Copper Touch Surfaces. http://www.coppertouchsurfaces.org/antimicrobial/bacteria/index.html (accessed 14 November 2016).

35 EPA. EPA registers copper-containing alloy products, http://www.epa.gov/pesticides/factsheets/copper-alloy-products.htm (accessed 14 November 2016).

36 Liao, K.-H., Ou, K.-L., Cheng, H.-C., Lin, C.-T., and Peng, P.-W. (2010) Effect of silver on antibacterial properties of stainless steel. *Appl. Surf. Sci.*, **256** (11), 3642–3646.

37 Huang, C.-F., Chiang, H.-J., Lan, W.-C., Chou, H.-H., Ou, K.-L., and Yu, C.-H. (2011) Development of silver-containing austenite antibacterial stainless steels for biomedical applications Part I: microstructure characteristics, mechanical properties and antibacterial mechanisms. *Biofouling*, **27** (5), 449–457.

38 Yang, K. and Lu, M. (2007) Antibacterial properties of an austenitic antibacterial stainless steel and its security for human body. *J. Mater. Sci. Technol.*, **23** (3), 333–336.

39 Nan, L., Liu, Y., Lue, M., and Yang, K. (2008) Study on antibacterial mechanism of copper-bearing austenitic antibacterial stainless steel by atomic force microscopy. *J. Mater. Sci. - Mater. Med.*, **19** (9), 3057–3062.

40 Nan, L., Yang, W., Liu, Y., Xu, H., Li, Y., Lu, M. *et al.* (2008) Antibacterial mechanism of copper-bearing antibacterial stainless steel against E.coli. *J. Mater. Sci. Technol.*, **24** (2), 197–201.

41 Nan, L. and Yang, K. (2010) Cu ions dissolution from Cu-bearing antibacterial stainless steel. *J. Mater. Sci. Technol.*, **26** (10), 941–944.

42 Nan, L., Cheng, J., and Yang, K. (2012) Antibacterial behavior of a Cu-bearing type 200 stainless steel. *J. Mater. Sci. Technol.*, **28** (11), 1067–1070.

43 Ren, L., Zhu, J., Nan, L., and Yang, K. (2011) Differential scanning calorimetry analysis on Cu precipitation in a high Cu austenitic stainless steel. *Mater. Des.*, **32** (7), 3980–3985.

44 Ren, L., Yang, K., Guo, L., and Chai, H.-w. (2012) Preliminary study of anti-infective function of a copper-bearing stainless steel. *Mater. Sci. Eng., C*, **32** (5), 1204–1209.

45 Ren, L., Nan, L., and Yang, K. (2011) Study of copper precipitation behavior in a Cu-bearing austenitic antibacterial stainless steel. *Mater. Des.*, **32** (4), 2374–2379.

46 Zhang, X., Huang, X., Ma, Y., Lin, N., Fan, A., and Tang, B. (2012) Bactericidal behavior of Cu-containing stainless steel surfaces. *Appl. Surf. Sci.*, **258** (24), 10058–10063.

47 Kang, M.K., Moon, S.K., Kwon, J.S., Kim, K.M., and Kim, K.N. (2012) Antibacterial effect of sand blasted, large-grit, acid-etched treated Ti-Ag alloys. *Mater. Res. Bull.*, **47** (10), 2952–2955.

48 Zhang, E., Li, F., Wang, H., Liu, J., Wang, C., Li, M. *et al.* (2013) A new antibacterial titanium–copper sintered alloy: preparation and antibacterial property. *Mater. Sci. Eng., C*, **33** (7), 4280–4287.

49 Robinson, D.A., Griffith, R.W., Shechtman, D., Evans, R.B., and Conzemius, M.G. (2010) In vitro antibacterial properties of magnesium metal against Escherichia coli, *P*seudomonas aeruginosa and *S*taphylococcus aureus. *Acta Biomater.*, **6** (5), 1869–1877.

50 Huang, L., Fozo, E.M., Zhang, T., Liaw, P.K., and He, W. (2014) Antimicrobial behavior of Cu-bearing Zr-based bulk metallic glasses. *Mater. Sci. Eng., C*, **39**, 325–329.

51 Lopez-Heredia, M.A., Sohier, J., Gaillard, C., Quillard, S., Dorget, M., and Layrolle, P. (2008) Rapid prototyped porous titanium coated with calcium phosphate as a scaffold for bone tissue engineering. *Biomaterials*, **29** (17), 2608–2615.

52 Balla, V.K., Bodhak, S., Bose, S., and Bandyopadhyay, A. (2010) Porous tantalum structures for bone implants: fabrication, mechanical and in vitro biological properties. *Acta Biomater.*, **6** (8), 3349–3359.

53 Ma, W., Wei, J.H., Li, Y.Z., Wang, X.M., Shi, H.Y., Tsutsumi, S. *et al.* (2008) Histological evaluation and surface componential analysis of modified micro-arc oxidation-treated titanium implants. *J. Biomed. Mater. Res. Part B*, **86** (1), 162–169.

54 Birch, M.A., Johnson-Lynn, S., Nouraei, S., Wu, Q.B., Ngalim, S., Lu, W.J. *et al.* (2012) Effect of electrochemical structuring of Ti6Al4V on osteoblast behaviour in vitro. *Biomed. Mater.*, **7** (3), 035016.

55 Chai, H.W., Guo, L., Wang, X.T., Gao, X.Y., Liu, K., Fu, Y.P. *et al.* (2012) In vitro and in vivo evaluations on osteogenesis and biodegradability of a ss-tricalcium phosphate coated magnesium alloy. *J. Biomed. Mater. Res. Part A*, **100A** (2), 293–304.

56 Hu, Y., Cai, K.Y., Luo, Z., Zhang, Y., Li, L.Q., Lai, M. *et al.* (2012) Regulation of the differentiation of mesenchymal stem cells in vitro and osteogenesis in vivo by microenvironmental modification of titanium alloy surfaces. *Biomaterials*, **33** (13), 3515–3528.

57 Lai, M., Cai, K., Hu, Y., Zhang, Y., Li, L., Luo, Z. *et al.* (2013) Construction of microenvironment onto titanium substrates to regulate the osteoblastic differentiation of bone marrow stromal cells in vitro and osteogenesis in vivo. *J. Biomed. Mater. Res. A*, **101** (3), 653–666.

58 Gotman, I., Ben-David, D., Unger, R.E., Bose, T., Gutmanas, E.Y., and Kirkpatrick, C.J. (2013) Mesenchymal stem cell proliferation and differentiation on load-bearing trabecular nitinol scaffolds. *Acta Biomater.*, **9** (9), 8440–8448.

59 Kim, J., Kim, H.N., Lim, K.T., Kim, Y., Pandey, S., Garg, P. *et al.* (2013) Synergistic effects of nanotopography and co-culture with endothelial cells on osteogenesis of mesenchymal stem cells. *Biomaterials*, **34** (30), 7257–7268.

60 Lee, Y.H., Bhattarai, G., Park, I.S., Kim, G.R., Kim, G.E., Lee, M.H. *et al.* (2013) Bone regeneration around N-acetyl cysteine-loaded nanotube titanium dental implant in rat mandible. *Biomaterials*, **34** (38), 10199–10208.

61 Lensing, R., Behrens, P., Muller, P.P., Lenarz, T., and Stieve, M. (2014) In vivo testing of a bioabsorbable magnesium alloy serving as total ossicular replacement prostheses. *J. Biomater. Appl.*, **28** (5), 688–696.

62 Qiao, Y., Zhang, W., Tian, P., Meng, F., Zhu, H., Jiang, X. *et al.* (2014) Stimulation of bone growth following zinc incorporation into biomaterials. *Biomaterials*, **35**, 6882–6897.

63 Menown, I.B.A., Noad, R., Garcia, E.J., and Meredith, I. (2010) The platinum chromium element stent platform: from alloy, to design, to clinical practice. *Adv. Ther.*, **27** (3), 129–141.

64 Scheller, B., Speck, U., Abramjuk, C., Bernhardt, U., Bohm, M., and Nickenig, G. (2004) Paclitaxel balloon coating, a novel method for prevention and therapy of restenosis. *Circulation*, **110** (7), 810–814.

65 Colombo, A., Drzewiecki, J., Banning, A., Grube, E., Hauptmann, K., Silber, S. *et al.* (2003) Randomized study to assess the effectiveness of slow- and moderate-release polymer-based paclitaxel-eluting stents for coronary artery lesions. *Circulation*, **108** (7), 788–794.

66 Park, S.J., Shim, W.H., Ho, D.S., Raizner, A.E., Park, S.W., Hong, M.K. *et al.* (2003) A paclitaxel-eluting stent for the prevention of coronary restenosis. *New Engl. J. Med.*, **348** (16), 1537–1545.

67 Ren, L., Xu, L., Feng, J., Zhang, Y., and Yang, K. (2012) In vitro study of role of trace amount of Cu release from Cu-bearing stainless steel targeting for reduction of in-stent restenosis. *J. Mater. Sci. - Mater. Med.*, **23** (5), 1235–1245.

68 Campos, C.M., Muramatsu, T., Iqbal, J., Zhang, Y.J., Onuma, Y., Garcia-Garcia, H.M. *et al.* (2013) Bioresorbable drug-eluting magnesium-alloy scaffold for treatment of coronary artery disease. *Int. J. Mol. Sci.*, **14** (12), 24492–24500.

69 Erbel, R., Di Mario, C., Bartunek, J., Bonnier, J., de Bruyne, B., Eberli, F.R. *et al.* (2007) Temporary scaffolding of coronary arteries with bioabsorbable magnesium stents: a prospective, non-randomised multicentre trial. *Lancet*, **369** (9576), 1869–1875.

70 Wittchow, E., Adden, N., Riedmuller, J., Savard, C., Waksman, R., and Braune, M. (2013) Bioresorbable drug-eluting magnesium-alloy scaffold: design and feasibility in a porcine coronary model. *Eurointervention*, **8** (12), 1441–1450.

71 Magnetic Resonance: a Peer-Reviewed, Critical Introduction. http://www.magnetic-resonance.org/ch/21-01.html (accessed 14 November 2016).

72 Li, H.Z. and Xu, J. (2014) MRI compatible Nb-Ta-Zr alloys used for vascular stents: optimization for mechanical properties. *J. Mech. Behav. Biomed. Mater.*, **32**, 166–176.

73 Shafiei, F., Honda, E., Takahashi, H., and Sasaki, T. (2003) Artifacts from dental casting alloys in magnetic resonance imaging. *J. Dent. Res.*, **82** (8), 602–606.

74 Nomura, S.N., Oya, K., Tanaka, Y., Kondo, R., Doi, H., Tsutsumi, Y. *et al.* (2010) Microstructure and magnetic susceptibility of as-cast Zr-Mo alloys. *Acta Biomater.*, **6** (3), 1033–1038.

75 Laurent, A. (1998) Materials and biomaterials for interventional radiology. *Biomed. Pharmacother.*, **52** (2), 76–88.

76 Ernstberger, T., Heidrich, G., and Buchhorn, G. (2007) Postimplantation MRI with cylindric and cubic intervertebral test implants: evaluation of implant shape, material, and volume in MRI artifacting – an in vitro study. *Spine J.*, **7** (3), 353–359.

77 Schenck, J.F. (1996) The role of magnetic susceptibility in magnetic resonance imaging: MRI magnetic compatibility of the first and second kinds. *Med. Phys.*, **23** (6), 815–850.

78 Nomura, N., Tanaka, Y., Suyalatu, Kondo, R., Doi, H., Tsutsumi, Y. *et al.* (2009) Effects of phase constitution of Zr-Nb alloys on their magnetic susceptibilities. *Mater. Trans.*, **50** (10), 2466–2472.

79 Suyalatu, Kondo, R., Tsutsumi, Y., Doi, H., Nomura, N., and Hanawa, T. (2011) Effects of phase constitution on magnetic susceptibility and mechanical properties of Zr-rich Zr-Mo alloys. *Acta Biomater.*, **7** (12), 4259–4266.

80 Kondo, R., Nomura, N., Suyalatu, Tsutsumi, Y., Doi, H., and Hanawa, T. (2011) Microstructure and mechanical properties of as-cast Zr-Nb alloys. *Acta Biomater.*, **7** (12), 4278–4284.

81 Kondo, R., Shimizu, R., Nomura, N., Doi, H., Suyalatu, Tsutsumi, Y. *et al.* (2013) Effect of cold rolling on the magnetic susceptibility of Zr-14Nb alloy. *Acta Biomater.*, **9** (3), 5795–5801.

82 Zhou, F.Y., Qiu, K.J., Li, H.F., Huang, T., Wang, B.L., Li, L. *et al.* (2013) Screening on binary Zr-1X (X = Ti, Nb, Mo, Cu, Au, Pd, Ag, Ru, Hf and Bi) alloys with good in vitro cytocompatibility and magnetic resonance imaging compatibility. *Acta Biomater.*, **9** (12), 9578–9587.

83 O'Brien, B., Stinson, J., and Carroll, W. (2008) Development of a new niobium-based alloy for vascular stent applications. *J. Mech. Behav. Biomed. Mater.*, **1** (4), 303–312.

84 O'Brien, B.J., Stinson, J.S., Boismier, D.A., and Carroll, W.M. (2008) Characterization of an NbTaWZr alloy designed for magnetic resonance angiography compatible stents. *Biomaterials*, **29** (34), 4540–4545.

85 Cheng, Y., Cai, W., Zheng, Y.F., Li, H.T., and Zhao, L.C. (2005) Surface characterization and immersion tests of TiNi alloy coated with Ta. *Surf. Coat. Technol.*, **190** (2-3), 428–433.

86 Narita, K., Niinomi, M., Nakai, M., Akahori, T., Tsutsumi, H., and Oribe, K. (2010) Bending fatigue and spring back properties of implant rods made of beta-type titanium alloy for spinal fixture. *Adv. Mater. Res.*, **89-91**, 400–404.

87 Nakai, M., Niinomi, M., Zhao, X., and Zhao, X. (2011) Self-adjustment of Young's modulus in biomedical titanium alloys during orthopaedic operation. *Mater. Lett.*, **65** (4), 688–690.

88 Zhao, X., Niinomi, M., Nakai, M., Miyamoto, G., and Furuhara, T. (2011) Microstructures and mechanical properties of metastable Ti-30Zr-(Cr, Mo) alloys with changeable Young's modulus for spinal fixation applications. *Acta Biomater.*, **7** (8), 3230–3236.

89 Zhao, X.F., Niinomi, M., Nakai, M., and Hieda, J. (2012) Beta type Ti-Mo alloys with changeable Young's modulus for spinal fixation applications. *Acta Biomater.*, **8** (5), 1990–1997.

90 Zhao, X.F., Niinomi, M., Nakai, M., Hieda, J., Ishimoto, T., and Nakano, T. (2012) Optimization of Cr content of metastable beta-type Ti-Cr alloys with

changeable young's modulus for spinal fixation applications. *Acta Biomater.*, **8** (6), 2392–2400.

91 Li, Q., Niinomi, M., Hieda, J., Nakai, M., and Cho, K. (2013) Deformation-induced omega phase in modified Ti-29Nb-13Ta-4.6Zr alloy by Cr addition. *Acta Biomater.*, **9** (8), 8027–8035.

92 Sumner, D.R., Turner, T.M., Igloria, R., Urban, R.M., and Galante, J.O. (1998) Functional adaptation and ingrowth of bone vary as a function of hip implant stiffness. *J. Biomech.*, **31** (10), 909–917.

93 Mantripragada, V.P., Lecka-Czernik, B., Ebraheim, N.A., and Jayasuriya, A.C. (2013) An overview of recent advances in designing orthopedic and craniofacial implants. *J. Biomed. Mater. Res. Part A*, **101** (11), 3349–3364.

94 Bayraktar, H.H., Morgan, E.F., Niebur, G.L., Morris, G.E., Wong, E.K., and Keaveny, T.M. (2004) Comparison of the elastic and yield properties of human femoral trabecular and cortical bone tissue. *J. Biomech.*, **37** (1), 27–35.

95 Rho, J.-Y., Tsui, T.Y., and Pharr, G.M. (1997) Elastic properties of human cortical and trabecular lamellar bone measured by nanoindentation. *Biomaterials*, **18** (20), 1325–1330.

96 Ueno, H., Kakihata, K., Kaneko, Y., Hashimoto, S., and Vinogradov, A. (2011) Enhanced fatigue properties of nanostructured austenitic SUS 316L stainless steel. *Acta Mater.*, **59** (18), 7060–7069.

97 Stolyarov, V.V., Zhu, Y.T., Alexandrov, I.V., Lowe, T.C., and Valiev, R.Z. (2001) Influence of ECAP routes on the microstructure and properties of pure Ti. *Mater. Sci. Eng. A*, **299** (1-2), 59–67.

98 Sergueeva, A.V., Stolyarov, V.V., Valiev, R.Z., and Mukherjee, A.K. (2001) Advanced mechanical properties of pure titanium with ultrafine grained structure. *Scr. Mater.*, **45** (7), 747–752.

99 Semenova, I.P., Yakushina, E.B., Nurgaleeva, V.V., and Valiev, R.Z. (2009) Nanostructuring of Ti-alloys by SPD processing to achieve superior fatigue properties. *Int. J. Mater. Res.*, **100** (12), 1691–1696.

100 Zheng, Y.F., Gu, X.N., and Witte, F. (2014) Biodegradable metals. *Mater. Sci. Eng., R*, **77**, 1–34.

101 Johnson, A.L., Houlton, J.E.F., and Vannini, R. (2005) *AO Principles of Fracture Management in the Dog and Cat*, Thieme, New York.

102 Ruedi, T.P. and Murphy, W.M. (2000) *AO Principles of Fracture Management*, 1st edn, Thieme, New York.

103 Mishnaevsky, L., Levashov, E., Valiev, R.Z., Segurado, J., Sabirov, I., Enikeev, N. *et al.* (2014) Nanostructured titanium-based materials for medical implants: modeling and development. *Mater. Sci. Eng., R*, **81**, 1–19.

104 Lü, X., Bao, X., Huang, Y., Qu, Y., Lu, H., and Lu, Z. (2009) Mechanisms of cytotoxicity of nickel ions based on gene expression profiles. *Biomaterials*, **30** (2), 141–148.

105 Stohs, S.J. and Bagchi, D. (1995) Oxidative mechanisms in the toxicity of metal ions. *Free Radical Biol. Med.*, **18** (2), 321–336.

106 Perl, D.P. and Brody, A.R. (1980) Alzheimer's disease: X-ray spectrometric evidence of aluminum accumulation in neurofibrillary tangle-bearing neurons. *Science*, **208** (4441), 297–299.

107 Walker, P.R., LeBlanc, J., and Sikorska, M. (1989) Effects of aluminum and other cations on the structure of brain and liver chromatin. *Biochemistry*, **28** (9), 3911–3915.

108 Landsberg, J.P., McDonald, B., and Watt, F. (1992) Absence of aluminium in neuritic plaque cores in Alzheimer's disease. *Nature*, **360** (6399), 65–68.

109 Sharma, M., Kumar, A.V.R., Singh, N., Adya, N., and Saluja, B. (2008) Electrochemical corrosion behavior of dental/implant alloys in artificial saliva. *J. Mater. Eng. Perform.*, **17** (5), 695–701.

110 Schiff, N., Grosgogeat, B., Lissac, M., and Dalard, F. (2004) Influence of fluoridated mouthwashes on corrosion resistance of orthodontics wires. *Biomaterials*, **25** (19), 4535–4542.

111 Assis, S.L., Wolynec, S., and Costa, I. (2006) Corrosion characterization of titanium alloys by electrochemical techniques. *Electrochim. Acta*, **51** (8–9), 1815–1819.

112 Fathi, M.H., Salehi, M., Saatchi, A., Mortazavi, V., and Moosavi, S.B. (2003) In vitro corrosion behavior of bioceramic, metallic, and bioceramic-metallic coated stainless steel dental implants. *Dent. Mater.*, **19** (3), 188–198.

113 Gu, X.N., Zheng, Y.F., Cheng, Y., Zhong, S.P., and Xi, T.F. (2009) In vitro corrosion and biocompatibility of binary magnesium alloys. *Biomaterials*, **30** (4), 484–498.

114 di Mario, C., Griffiths, H., Goktekin, O., Peeters, N., Verbist, J., Bosiers, M. *et al.* (2004) Drug-eluting bioabsorbable magnesium stent. *J. Interv. Cardiol.*, **17** (6), 391–395.

115 Böse, D., Eggebrecht, H., Haude, M., Schmermund, A., and Erbel, R. (2006) First absorbable metal stent implantation in human coronary arteries. *Am. Heart Hosp. J.*, **4** (2), 128–130.

116 Witte, F. (2010) The history of biodegradable magnesium implants: a review. *Acta Biomater.*, **6** (5), 1680–1692.

117 Peuster, M., Wohlsein, P., Brügmann, M., Ehlerding, M., Seidler, K., Fink, C. *et al.* (2001) A novel approach to temporary stenting: degradable cardiovascular stents produced from corrodible metal – results 6–18 months after implantation into New Zealand white rabbits. *Heart*, **86** (5), 563–569.

118 Heublein, B., Rohde, R., Kaese, V., Niemeyer, M., Hartung, W., and Haverich, A. (2003) Biocorrosion of magnesium alloys: a new principle in cardiovascular implant technology? *Heart*, **89** (6), 651–656.

119 Zartner, P., Cesnjevar, R., Singer, H., and Weyand, M. (2005) First successful implantation of a biodegradable metal stent into the left pulmonary artery of a preterm baby. *Catheter. Cardiovasc. Interventions*, **66** (4), 590–594.

120 Schranz, D., Zartner, P., Michel-Behnke, I., and Akintürk, H. (2006) Bioabsorbable metal stents for percutaneous treatment of critical recoarctation of the aorta in a newborn. *Catheter. Cardiovasc. Interventions*, **67** (5), 671–673.

121 Peeters, P., Bosiers, M., Verbist, J., Deloose, K., and Heublein, B. (2005) Preliminary results after application of absorbable metal stents in patients with critical limb ischemia. *J. Endovasc. Ther.*, **12** (1), 1–5.

122 Bosiers, M., Peeters, P., D'Archambeau, O., Hendriks, J., Pilger, E., Duber, C. *et al.* (2009) AMS INSIGHT – absorbable metal stent implantation for

treatment of below-the-knee critical limb ischemia: 6-month analysis. *Cardiovasc. Interventional Radiol.*, **32** (3), 424–435.

123 Derby, B. (2012) Printing and prototyping of tissues and scaffolds. *Science*, **338** (6109), 921–926.

124 Tarnita, D., Berceanu, C., and Tarnita, C. (2010) The three-dimensional printing – a modern technology used for biomedical prototypes. *Mater. Plast.*, **47** (3), 328–334.

125 Hutmacher, D.W. (2000) Scaffolds in tissue engineering bone and cartilage. *Biomaterials*, **21** (24), 2529–2543.

126 Sachs, E., Cima, M., Williams, P., Brancazio, D., and Cornie, J. (1992) 3-Dimensional printing – rapid tooling and prototypers directly from a cad model. *J. Eng. Ind-T ASME*, **114** (4), 481–488.

127 Wu, B.M., Borland, S.W., Giordano, R.A., Cima, L.G., Sachs, E.M., and Cima, M.J. (1996) Solid free-form fabrication of drug delivery devices. *J. Control. Release*, **40** (1-2), 77–87.

128 Biesiekierski, A., Wang, J., Gepreel, M.A., and Wen, C. (2012) A new look at biomedical Ti-based shape memory alloys. *Acta Biomater.*, **8** (5), 1661–1669.

129 Valiev, R.Z., Islamgaliev, R.K., and Alexandrov, I.V. (2000) Bulk nanostructured materials from severe plastic deformation. *Prog. Mater Sci.*, **45** (2), 103–189.

130 Stolyarov, V.V., Zhu, Y.T., Lowe, T.C., Islamgaliev, R.K., and Valiev, R.Z. (1999) A two step SPD processing of ultrafine-grained titanium. *Nanostruct. Mater.*, **11** (7), 947–954.

131 Agnew, S.R., Horton, J.A., Lillo, T.M., and Brown, D.W. (2004) Enhanced ductility in strongly textured magnesium produced by equal channel angular processing. *Scr. Mater.*, **50** (3), 377–381.

132 Valiev, R.Z. and Langdon, T.G. (2006) Principles of equal-channel angular pressing as a processing tool for grain refinement. *Prog. Mater Sci.*, **51** (7), 881–981.

133 Zhilyaev, A.P. and Langdon, T.G. (2008) Using high-pressure torsion for metal processing: fundamentals and applications. *Prog. Mater Sci.*, **53** (6), 893–979.

134 Sakai, G., Nakamura, K., Horita, Z., and Langdon, T.G. (2005) Developing high-pressure torsion for use with bulk samples. *Mater. Sci. Eng. A*, **406** (1-2), 268–273.

135 Valiev, R.Z., Ivanisenko, Y.V., Rauch, E.F., and Baudelet, B. (1996) Structure and deformation behaviour of Armco iron subjected to severe plastic deformation. *Acta Mater.*, **44** (12), 4705–4712.

136 Valiev, R.Z., Zehetbauer, M.J., Estrin, Y., Hoeppel, H.W., Ivanisenko, Y., Hahn, H. *et al.* (2007) The innovation potential of bulk nanostructured materials. *Adv. Eng. Mater.*, **9** (7), 527–533.

137 Hoppel, H.W., May, J., and Goken, M. (2004) Enhanced strength and ductility in ultrafine-grained aluminium produced by accumulative roll bonding. *Adv. Eng. Mater.*, **6** (9), 781–784.

138 Perez-Prado, M.T., del Valle, J.A., and Ruano, O.A. (2004) Grain refinement of Mg-Al-Zn alloys via accumulative roll bonding. *Scr. Mater.*, **51** (11), 1093–1097.

139 Saito, Y., Tsuji, N., Utsunomiya, H., Sakai, T., and Hong, R.G. (1998) Ultra-fine grained bulk aluminum produced by accumulative roll-bonding (ARB) process. *Scr. Mater.*, **39** (9), 1221–1227.

140 Saito, Y., Utsunomiya, H., Tsuji, N., and Sakai, T. (1999) Novel ultra-high straining process for bulk materials – development of the accumulative roll-bonding (ARB) process. *Acta Mater.*, **47** (2), 579–583.

141 Yamashita, A., Horita, Z., and Langdon, T.G. (2001) Improving the mechanical properties of magnesium and a magnesium alloy through severe plastic deformation. *Mater. Sci. Eng., A*, **300** (1–2), 142–147.